A cumulative damage model for extremely low cycle fatigue cracking in steel structure

Xuewei Huang[a] and Jun Zhao[*]

School of Mechanics and Engineering Science, Zhengzhou University, No.100, Science Avenue, Zhengzhou 450001, China

Abstract. The purpose of this work is to predict ductile fracture of structural steel under extremely low cyclic loading experienced in earthquake. A cumulative damage model is proposed on the basis of an existing damage model originally aiming to predict fracture under monotonic loading. The cumulative damage model assumes that damage does not grow when stress triaxiality is below a threshold and fracture occurs when accumulated damage reach unit. The model was implemented in ABAQUS software. The cumulative damage model parameters for steel base metal, weld metal and heat affected zone were calibrated, respectively, through testing and finite element analyses of notched coupon specimens. The damage evolution law in the notched coupon specimens under different loads was compared. Finally, in order to examine the engineering applicability of the proposed model, the fracture performance of beam-column welded joints reported by previous researches was analyzed based on the cumulative damage model. The analysis results show that the cumulative damage model is able to successfully predict the cracking location, fracture process, the crack initiation life, and the total fatigue life of the joints.

Keywords: cumulative damage model; structural steel; extremely low cycle fatigue; ductile fracture; beam-column welded joint

1. Introduction

Extreme loads applied to steel structures can result in fatigue failure at very small number of cycles. This fatigue regime is called extremely low cycle fatigue (ELCF) or ultra low cycle fatigue (Kuroda 2002, Kamaya 2010, Nip *et al.* 2010). As an example, the steel building structures were typically subjected to extremely low cyclic loading during strong seismic action, and this type of fracture in steel frame structure were observed in the strong earthquake (Mahin 1998, Kuwamura 1998). The extremely low cycle fatigue is characterized by very few loading cycles (commonly less than 20 cycles) and large inelastic strain amplitude (Bleck *et al.* 2009, Amiri *et al.* 2013). ELCF is quite different from conventional high (or low) cycle fatigue, which leads to large plastic strains resulting in a ductile crack in place of a fatigue crack. In addition, the fracture modes are also different between ELCF and high (or low) cycle fatigue. For instance, in several pull-push round bar fatigue tests, the crack often initiates in the interior of specimen in the ELCF range, while the fatigue crack originates from the surface in the high cycle fatigue or low cycle fatigue regime (Kamaya 2010). The micro-mechanism underlying the ELCF consists of voids nucleation, continuous growth and finally coalescence (Dufailly and Lemaitre 1995), which are closely associated with the ductile fracture under monotonic loading. Voids nucleation occurs due to debonding of inclusions from the metal matrix. During the growth stage, the nucleated voids growth depends on existing stress state and plastic strain. Void coalescence is the final stage which leads to ductile crack initiation.

There is a growing interest in the modelling of ELCF fracture under earthquake loading. From engineering perspective, the final aim of application of fracture prediction models is to access the fracture vulnerability of critical components (Chao *et al.* 2006) and predict the collapse performance of structural steel (Li *et al.* 2015), and then to avoid the ductile fracture initiation in the design of structure steel components (Myers *et al.* 2009a). In the present, the ELCF fracture model can be categorized into two groups: coupled models and uncoupled models. The coupled models are able to describe the variation of material microstructure during the fracture process, which can be broadly divided into micromechanical-based (Leblond *et al.* 1995, Ristinmaa 1997, Besson and Guillemer 2003) and damage-based models (Pirondi and Steglich 2003, Steglich *et al.* 2005). The micromechanical-based models are developed on the basis of the void growth in plastic media while the damage-based models simulate the void evolution by introducing internal variables into constitutive equations. The coupled models have been verified to simulate ELCF initiation in notched coupon specimens (Pirondi *et al.* 2006) and ELCF failure of beam-column welded joint (Huang *et al.* 2013, Tong *et al.* 2016). However, coupled models have a high computational cost, and the model calibration is complex. As an example, nine model parameters is required to be calibrated for Gurson-type model and the computational cost is very high,

---

∗Corresponding author, Professor
 E-mail: zhaoj_zzu@126.com
[a]Lecturer
 E-mail: huangxw_zzu@126.com

furthermore, the calibration process depends on individual experiences and model parameters are found to be non-unique.

Regarding uncoupled models, the stress and strain history are used to describe critical conditions for fracture initiation. These models often adopted the standard J_2 plastic theory and ignored the effect of damage on the constitutive model. Kuroda (2002) developed a cumulative damage model to predict ELCF life. This model was presented based on the notion that the damage resulting from ductility exhaustion is the dominant factor at the large level of plastic strain amplitude, while the damage resulting from crack growth is the dominant factor at the small level of plastic strain amplitude. Xue (2008) proposed a new expression to capture the cyclic life over the entire span of ELCF to LCF by introducing an exponential function. However, these models above mentioned do not consider the effect of stress state and their application are limited to material scale. The cyclic void growth model (CVGM) grounded on the cyclic behavior of microvoid, proposed by Kanvinde and Deierlein (2007) can also be classed as an uncoupled model, which was originally presented to predict ductile fracture in the case of monotonic loading (Kanvinde and Deierlein 2006a). The model is able to account for the influence of complex stress-strain state on fracture prediction. The accuracy of the CVGM was demonstrated by a multitude of experiments and numerical investigations of blunt notched compact tension specimens and dog bone steel specimens (Kanvinde and Deierlein 2008). Moreover, the application to the steel column baseplate joints (Myers 2009b) and beam-column welded joints (Zhou *et al.* 2013, 2014) has shown ability of the CVMG model for predicting ductile fracture in structural steel. Kiran and Khandelwal (2015) examined the effect of stress triaxiality and Lode parameter on void deformation under extremely low cyclic loading condition, and a new micromechanical cyclic void growth model was developed to estimate the fatigue life of ASTM A992 steels.

The research aims to introduce a new cumulative damage model for predicting ELCF fracture in steel structures. The cumulative damage model is extended from the damage model under monotonic loading, which is also considered as an uncoupled model. The damage evolution and fracture initiation of notched coupon specimens under different loading condition are investigated. Moreover, ELCF performance of beam-column welded joints is evaluated using the damage model. This provides considerable insight into the complicated fracture behavior of joints.

2. Damage model for extremely-low-cycle-fatigue fracture

Ductile fracture is driven by growth and coalescence of voids. Rice and Tracey (1969) argued that the growth of void was related to both of the plastic strains and the triaxial stresses. The model is referred to as void growth model (VGM). Based on VGM model, one simplified model, named as stress modified critical strain (SMCS) model, was developed by Hancock and Mackenzie (1976) and further studied by Rousselier (1987), Kanvinde and Deierlein (2006a, 2006b). Ductile crack is triggered when accumulated plastic strain reaches the critical value. The critical accumulated plastic strain is calculated as follows

$$\varepsilon_p^{critical} = \alpha \exp(-1.5T) \tag{1}$$

where T is the stress triaxiality which is the ratio between the mean stress σ_m and the von Mises equivalent stress σ_e. α is a material constant. $\varepsilon_p = \int \sqrt{(2/3) d\varepsilon_{ij}^p \bullet d\varepsilon_{ij}^p}$, $d\varepsilon_{ij}^p$ is matrix plastic strain tensor increment. It is assumed that the ductile crack initiates when the void coalesce over a characteristic length (l^*) which is another parameter to be calibrated in the SMCS model. In the previous research, scanning electron microscope was used to measure the characteristic length in the fracture surface of specimen (Mackenzie 1977, Kanvinde and Deierlein 2006a).

Once the form of $\varepsilon_p^{critical}$ is available as a function of the stress triaxiality, the power law damage rule can be defined by the following equation

$$D = \left(\frac{\varepsilon_p}{\alpha \exp(-1.5T)} \right)^m \tag{2}$$

where m is the damage exponent. The parameter determined the shape of damage evolution rule with plastic strain, which reflect the different void nucleation and growth process. Fig. 1 shows three possible accumulated damage evolution rules with three different value of the m exponent. In particular, when the value of m is larger than 1.0, the damage curve is the behavior of materials where few new voids in the material can be nucleated with the increase of plastic strain. Thus the existing voids growth leads to a low initial damage accumulated rate. When the growing plastic strain exceeds the critical value, rapid void coalescence begins to occur. These processes are often observed in steel metal. As for the value of m smaller than 1.0, the damage initially accumulated rapidly due to the nucleation of plenty of small voids as plastic strain increases, which is observed in the test of Al and Al-Li alloy (Bonora 1997). Once the nucleation process is saturated, the void grows with a consequent constant speed, the increasing plastic strain leads to void coalescence. Finally, when m equals to 1.0, the damage evolution law can be expressed as linear law. The whole failure process is a combination of void nucleation and void growth.

During the loading history, equivalent plastic distortion ε_d, defined on plastic strain component, represents the current plastic strain state, i.e.

$$\varepsilon_d = \frac{\sqrt{2}}{3} \sqrt{\left(\varepsilon_1^p\right)^2 + \left(\varepsilon_2^p\right)^2 + \left(\varepsilon_3^p\right)^2} \tag{3}$$

where ε_1^p, ε_2^p and ε_3^p are the three principal plastic strain components. It is noted that equivalent plastic distortion is different to the accumulated plastic strain ε_p, which captures the effect of plastic strain history during loading process. However, under monotonic loading condition, the incremental equivalent plastic distortion
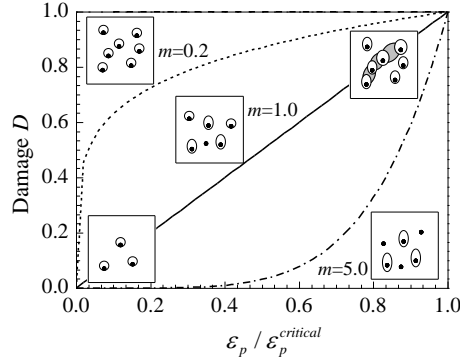
Fig. 1 Different damage evolution rules with different value of the *m* exponent

Fig. 2 Dimension of notched coupon specimen (Liao *et al.* 2012)

equal to incremental equivalent plastic distortion for each proportional loading branch. The damage growing rate can be rewritten by the following equation based on Eq. (2)

$$\mathrm{d}D = m\left(\frac{\varepsilon_p}{\alpha\exp(-1.5T)}\right)^{m-1}\frac{1}{\alpha\exp(-1.5T)}\mathrm{d}\varepsilon_p \qquad (4)$$

or to expressed as the function of equivalent plastic distortion, i.e.

$$\mathrm{d}D = m\left(\frac{\varepsilon_d}{\alpha\exp(-1.5T)}\right)^{m-1}\frac{1}{\alpha\exp(-1.5T)}\mathrm{d}\varepsilon_d \qquad (5)$$

The mechanism of extremely low cycle fatigue is demonstrated by void growth and coalescence, and therefore it is rational to extend the damage evolution model suitable for monotonic loading to the case of extremely low cycle fatigue with some hypotheses. Under cyclic loading, the stress state of material can be described by the variable of stress triaxiality (Pirondi and Bonora 2003). The positive stress triaxiality means that the material is subjected to tension load while the negative stress traixiality means that the material is in compression. The primary difference between ELCF fracture and monotonic tension fracture is that negative stress triaxiality are involved at cracked regions under ELCF loading, and it is indispensable to investigate the damage evolution rule under negative stress triaxiality.

For monotonic loading, Bao and Wierzbicki (2004, 2005) analyze a host of test results under negative stress triaxiality *T*. It is indicated that there is a cutoff value of *T* i.e., -1/3. If stress triaxiality *T* is below -1/3, the material will not fracture under monotonic tension or compression loading condition. The voids nucleation may not happen under monotonic compression loading condition, thus damage does not accumulate when *T* is below -1/3. However, the damage evolution rule as the stress triaxiality is less than -1/3 under ELCF loading might be some difference. Under negative stress triaxiality, the material is subjected to compression loading, the voids are able to change their shapes when the material is subjected to ELCF loading condition, and the damage will probably grow because of the void shape change when stress triaxiality is less than -1/3. However, so far, the mechanism is still an open question when stress triaxiality is less than zero,
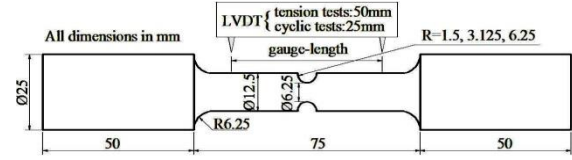
especially for ELCF. In accordance with the round bar tensile test results of Besson *et al.* (2001), the voids can only be observed at the instants close to the fracture point, which means that the void sizes can be negligible at most strain amplitudes. Besides, high positive stress triaxiality regime is commonly encountered in engineering applications, and the ductile failure is dominated by void growth and void coalescence due to necking of intervoid ligaments (Kiran and Khandelwal 2014). Therefore, this article assumes that if *T* is less than -1/3 in ELCF loading, damage will not cumulate within the most strain amplitudes expect those close to the fracture stain, and a new variable named as active equivalent plastic distortion increment $\mathrm{d}\varepsilon_d^+$ is defined as

$$\mathrm{d}\varepsilon_d^+ = \begin{cases} \mathrm{d}\varepsilon_d & T > -1/3 \\ 0 & T \le -1/3 \end{cases} \qquad (6)$$

It can be observed from Eq. (6) that the active equivalent plastic distortion increment is equal to the equivalent plastic distortion increment when *T* is above -1/3. Then the damage evolution law under extremely low cyclic loading can be written as

$$\mathrm{d}D = m\left(\frac{\varepsilon_d^+}{\alpha\exp(-1.5T)}\right)^{m-1}\frac{1}{\alpha\exp(-1.5T)}\mathrm{d}\varepsilon_d^+ \qquad (7)$$

It is to be noted that Eq. (7) is able to degenerate to Eq. (5) when the material is subjected to monotonic loading, therefore, the cumulative damage model as expressed by Eq. (7) can also be used under monotonic loading and ELCF loading.

3. Damage model calibration

3.1 Materials

A common structural steel Q345, which is extensive applied in building steel structures of China, is selected to be analyzed in this study. Besides, the corresponding weld metal and weld heat affected zone metal are also investigated. The notched coupon specimens extracted from a welded joint were tested by Liao *et al.* (2012). Fig. 2 illustrates the geometries and dimensions of notched specimens. In order to obtain a large range of stress triaxiality, three different notch radius specimens were provided for each material. Axial displacement was monitored in the test by using of displacement meter with the gauge length of 50 mm for monotonic loading and 25 mm for extremely low cyclic loading.
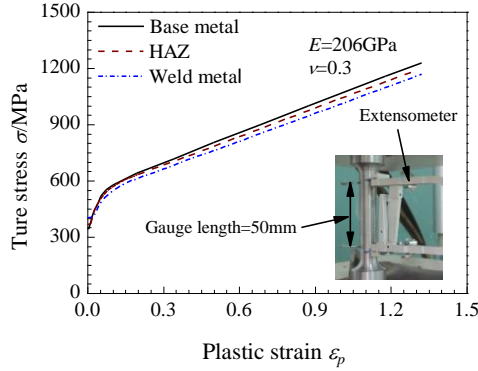
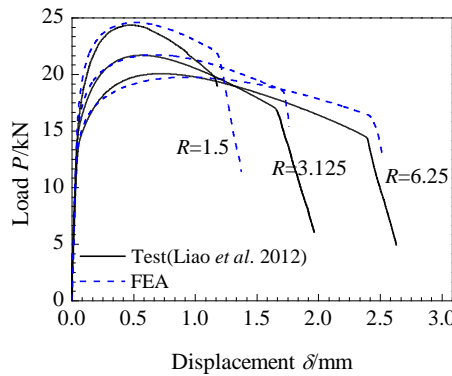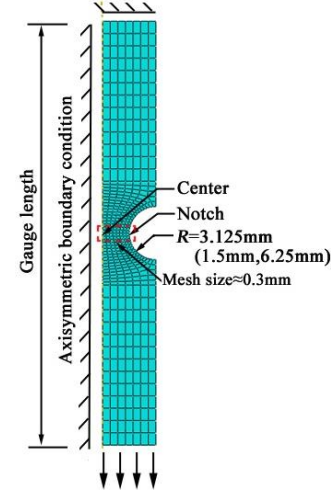Fig. 3 Material true stress-plastic strain characteristics

Fig. 4 Comparison of load displacement curves from experiment and finite element analysis for base metal

3.2 Calibration of material parameter α

Based on the standard tensile tests of smooth specimens conducted by Liao *et al.* (2012), the true stress strain curves is obtained according to the method presented by Huang *et al.* (2013), which are plotted in Fig. 3. Fig. 4 shows the tested load versus displacement curves of base metal notched specimens. It can be found that, as the notch radius decreases, the displacement to fracture decreases due to the higher stress triaxialties introduced by the notch.

In order to obtain the material parameter α in the SMCS model, elastic-plastic finite element calculations were carried out using the software ABAQUS to analyze the notched coupon specimen under tensile tests. Due to symmetry, two dimensional axisymmetric finite element models within gauge length were modeled for the notched specimens. The hardening curves illustrated in Fig. 3 were employed in the finite element analysis (FEA) and geometric nonlinearities were also considered. A typical finite element model of notched coupon specimens is manifested in Fig.5. The mesh size in the notch area was set to approximately 0.3mm, which was comparable to the material characteristic length l^* measured by Liao *et al.* (2012).

As shown in Fig. 4, a significant load drop appears in the final stage of load displacement curves in experiments. This drop is treated as the instance of ductile cracking in this work. Actually, even if crack begins to appear in the specimens, the load could still increase due to hardening behavior of materials. But the experimental results indicate

that crack propagates very quickly in the specimens. Consequently, it is rational that the initiation point of load drop is taken as an approximate indication of the onset of cracking. In addition, the test results (Liao *et al.* 2012) show that crack originated from the center for all notched specimens. The relationship between stress triaxiality and accumulated plastic strain in the center of specimen can be obtained from the FEA for each notched specimen. Then, the relationships corresponding to fracture initiation were substituted into Eq. (1) to inverse computation of the material parameter α. This calibration method based on test results and FEA to calculate the material parameter α was conducted for each notched coupon specimen. Table 1 lists the final calibrated results of parameter α.

3.3 Calibration of material parameter m

ELCF tests of notched coupon specimens were carried out by Liao *et al.* (2012). The cyclic loading histories fall into two categories which are named as CTF and C-PTF respectively, as shown in Fig. 6. For CTF loading history, the predetermined constant displacement amplitude was applied on the notched coupon specimens until rupture occurs. As for C-PTF loading history, the specimens firstly experienced five cycles of lower displacement amplitudes, and then subjected to a monotonic tension loading till fracture.

Fig. 5 Finite element model of notched specimens (*R*=3.125 mm)

Table 1 Calibration of parameter α in SMCS model

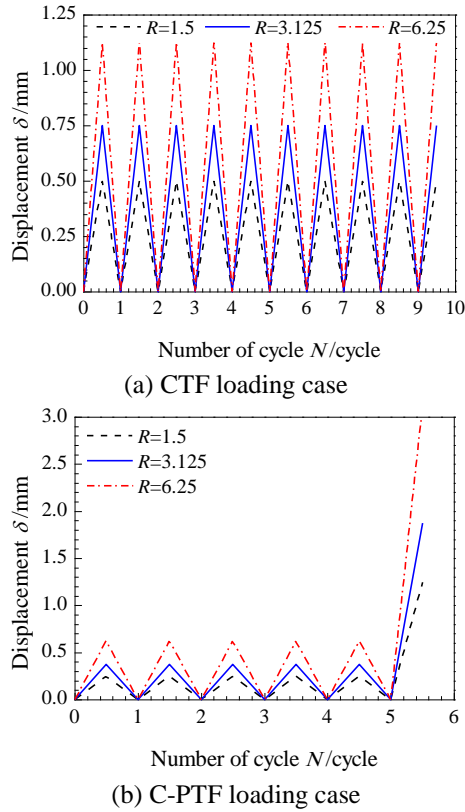| Material	Base metal		Weld metal		Heat zone metal	
Notch radius *R*/mm	No.	α	No.	α	No.	α
1.5	4-1	-	4-2	2.89	4-3	2.33
	5-1	2.90	5-2	2.92	5-3	2.91
3.125	10-1	2.19	10-2	2.21	10-3	2.35
	11-1	2.25	11-2	1.92	11-3	2.06
6.25	16-1	2.50	16-2	2.41	16-3	2.17
	17-1	2.56	17-2	2.28	17-3	1.91
Average		2.47		2.46		2.34

(a) CTF loading case

(b) C-PTF loading case

Fig. 6 Extremely low cyclic loading histories of notched coupon specimens (Liao *et al.* 2012)

The finite element mesh of notched specimens under ELCF loading is identical with that used under monotonic loading, as shown in Fig. 5. The inelastic cyclic behavior of base metal, weld metal and heat affect zone metal is modeled using nonlinear mixed isotropic kinematic hardening constitutive model. From the previous researches, the hardening model parameters were calibrated by Huang *et al.* (2013), and the true stress strain curves shown in Fig. 3 could also be described by the hardening model parameters. Fig. 7 compares the test results and finite element results in the term of load displacement curve for the quintessential notched specimens (*R*=6.25 mm) of base metal. It shows that the numerical predictions are close to the test results till the crack onset where bearing capacity is abruptly lost. The fracture initiation of the notched specimens can't be predicted due to no damage incorporated into hardening model. Under ELCF loading, the test results show that crack initiated in the center of the specimens for all notched coupon specimens, which is also observed in the monotonic loading tests.

For the cumulative damage model shown in Eq. (7), the parameter α for base metal, weld metal and HAZ metal have been given in Table 1. The damage becomes the critical value, D_{cr}, when ductile fracture is assumed over the characteristic length, and the critical value is theoretically equal to one.

Therefore the damage exponent m is only parameter to be calibrated in the next. For a given notched specimen, accumulated damage reaches the critical value in the center of the specimen over the strain history when crack initiation
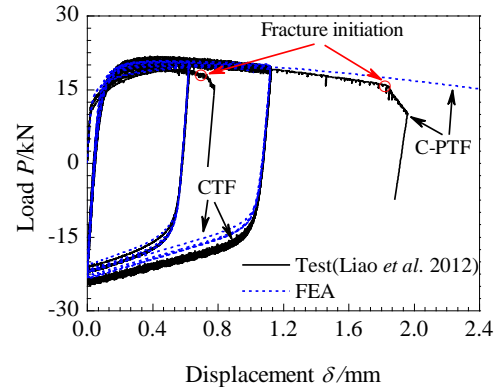

Fig. 7 Load versus displacement curves of base metal notched specimens (*R*=6.25 mm)

obtained from the experiment. The value of exponent m is evaluated to best match this condition. The calibrated results of m for all notched coupon specimens are summarized in Table 2. The mean value of damage exponent m is 2.47 for Q345 base metal. This damage exponent can be considered as a model parameter of material. Based on this calibration method and the test data provided by Kanvinde and Deierlein (2006a, 2007) and Myers (2009a), the damage exponent m of AW50 steel and JW50 steel are determined as 1.33 and 2.60 in this study, while the value of α of both materials equal to 2.59 and 4.23, respectively, which are given by Kanvinde and Deierlein (2006a).

4. Damage evolution of notched coupon specimens

In order to analyze the damage evolution of the previously mentioned tested notched coupon specimens, the detailed numerical simulation were performed in this section. Axisymmetric models using CAX4R elements were employed in the finite element calculation, and the typical model as displayed in Fig. 5 was established using ABAQUS software. Quasi-static analysis method was conducted in the explicit module to predict the rupture of the notched specimens under monotonic loading and ELCF loading condition. The explicit module adopts explicit integration programme to tackle advanced nonlinear complex problems, such as dynamic, contact and failure events. Increasing the step time is a convenient way to assure finite element calculation quasi-static, where the kinematic energy was smaller than 5% of the internal energy for each model. Furthermore, the notched specimen tensile tests were simulated using hardening model parameters of the corresponding materials (Huang *et al.* 2013), combined with the proposed cumulative damage model. In this study, both the hardening model and the damage model were implemented into ABAQUS software by means of the user-defined material subroutine. For fracture prediction of structure, element can be considered as failure in numerical simulation when accumulated damage equal to critical damage, and then the stress of failure element releases and numerical calculation is performed on the basis of the new damage state of structure.

Table 2 Calibration of damage exponent *m*

Material		Base metal		Weld metal		Heat zone metal	
Notch radius /mm	Loading case	Specimen No.	*m*	Specimen No.	*m*	Specimen No.	*m*
R=1.5	CTF	6-1	–	6-2	2.89	6-3	2.33
		7-1	2.90	7-2	2.92	7-3	2.91
	C-PTF	8-1	2.65	8-2	2.84	8-3	-
		9-1	2.67	9-2	2.98	9-3	-
R=3.125	CTF	12-1	2.19	12-2	2.21	12-3	2.35
		13-1	2.25	13-2	1.92	13-3	2.06
	C-PTF	14-1	–	14-2	2.38	14-3	2.03
		15-1	2.45	15-2	2.31	15-3	1.78
R=6.25	CTF	18-1	2.50	18-2	2.41	18-3	2.17
		19-1	2.56	19-2	2.28	19-3	1.91
	C-PTF	20-1	2.15	20-2	2.21	20-3	2.95
		21-1	2.35	21-2	2.19	21-3	2.91
Average		2.47		2.46		2.34	

The similar calculation is to be continued up to the fracture fail of structure. Crack propagation path is able to be predicted in the light of the sequence of reaching critical damage of elements.

Fig. 4 and Fig. 8 compare the predicated and tested load displacement curves for the quintessential notched specimens subjected to tensile loading and ELCF loading. It can be found that the predicted fracture initiation point agree with the experimental results. This is not surprising as the parameters associated with the new cumulative damage model are determined according to notched coupon specimen tensile and cyclic data, as explained in Section 3. It is noted that the load in the numerical results of all the notched coupon specimens is slightly higher than that in the experimental results at the part close the fracture displacement. The reason may be lie in that the standard J_2 plasticity theory applied in the finite element simulation is not able to represent material deterioration behavior.

The damage evolution law at two critical locations, i.e. in the center and at the notch of specimens for base metal, is plotted in Fig. 9. It indicates that damage reached the critical value earlier in the center of notched specimens as compared to that in the notch root, thus crack initiated in the coupon specimen's center, which agree with the test results. In Eq. (7), it shows that there are two competing factors in the damage model, stress triaxiality *T* and active equivalent plastic distortion ε_d^+, which promote the fracture initiation. Fig. 10 shows the profiles of stress triaxiality *T* and active equivalent plastic distortion ε_d^+ when fracture is initiated, while Fig. 11 shows the damage distribution profile. In the case of 6.25 mm notch radius, ε_d^+ developed simultaneously across the whole section and *T* was maximum in the center of specimen, and therefore the damage dropped from the center to the notch shown in Fig. 11. As for 1.5mm notch radius, the higher *T* in the center prevails on higher ε_d^+ at the notch, and therefore the first element reaches critical damage in the center of notched coupon specimen.
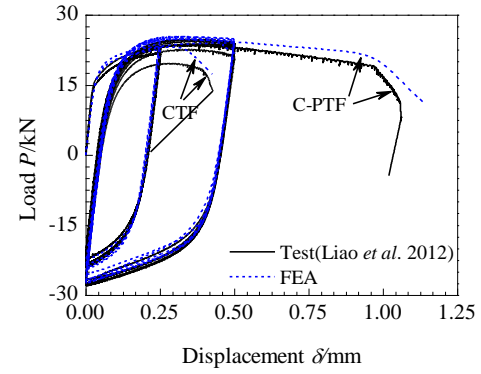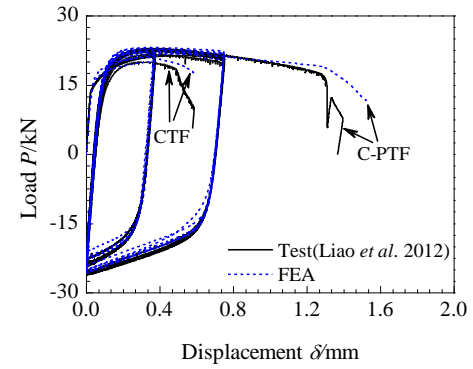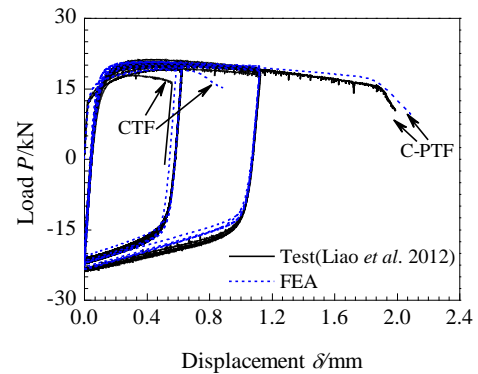

(a) *R*=1.5 mm

(b) *R*=3.125 mm

(c) *R*=6.25 mm

Fig. 8 Tested load displacement curves with simulated results for HAZ metal

In order to further analyze the competition between *T* and ε_d^+ for the notched coupon specimens, the fracture locus of specimens with different notch radius were predicted using the new cumulative damage model. Fig. 12 shows the damage distribution when fracture is initiated. It can be seen that the fracture initiation location is in the center for the blunter notched specimen, whereas fracture initiation location is at the notch for the sharper notched specimen. It can be proved by both typical mechanics experiments. One is fracture mechanics tests, sharper notched is similar to the initial crack, thereby crack initiated at the notch of coupon specimen. The other is the standard coupon specimens tensile tests, the uniform stress distribution at the notch section for the blunter notched specimens is comparable to that in the standard coupon specimens, thus ductile failure initiation is expected to
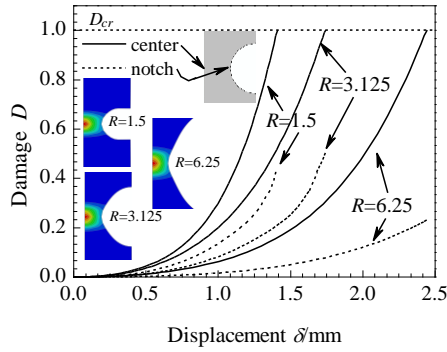
Fig. 9 Damage evolution law in the center of specimen and at the notch root for base metal
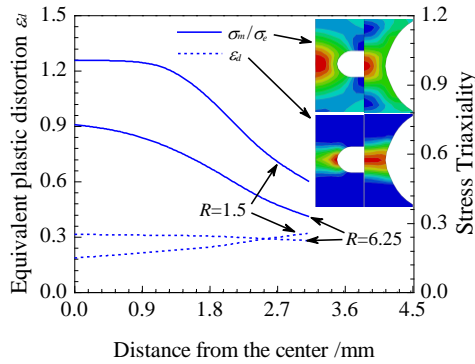

Fig. 10 Variation of ε_d and stress triaxiality across notched section for base metal
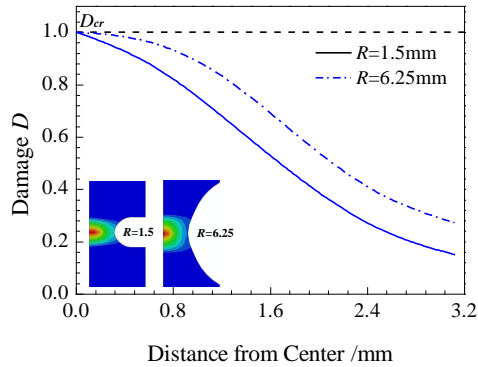

Fig. 11 Variation of damage across the notched section for base metal
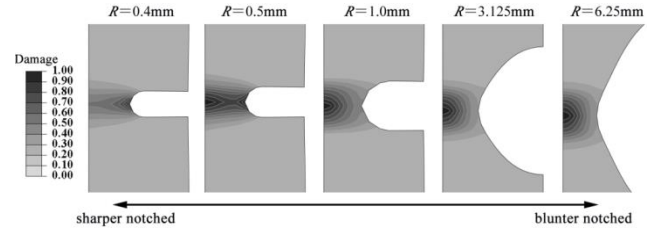

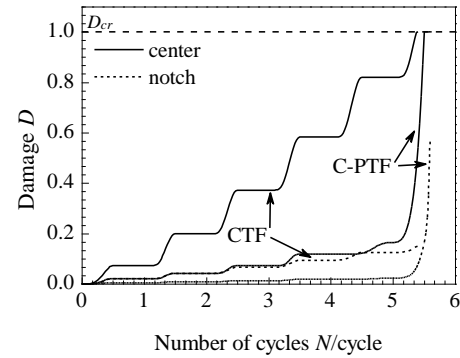Fig. 12 Fracture initiation locations predicted by finite element results

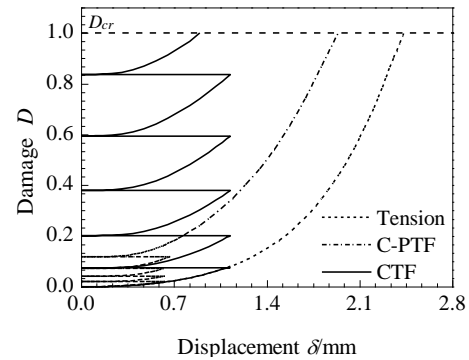Fig. 13 The damage evolution law at the different location of notched specimen for base metal (R=6.25 mm)

Fig. 14 The damage evolution law in the center of base metal specimen subjected to different loading conditions (R=6.25 mm)

occur at the specimen center. Besides, for the base metal notched coupon specimens with the notch radius 0.5mm, crack initiated at notch root and center at the same time, as shown in Fig. 12.

For the sake of facilitate understanding of the damage evolution law under extremely low cyclic loading, Fig. 13 provides an example of the finite element results of the damage at the notch and in the center as a function of loading cycles in the case of base metal notched specimen (R=6.25 mm). It indicates that the damage increases as loading cycles increase. The platform in Fig. 13 represents the phenomenon that damage accumulate rate is equal to zero under elastic unloading or stress triaxiality below -1/3. In addition, damage is generally higher in the center

compared to the notch root. It implies that crack initiation region located in the center of specimens for the base metal notched specimens subjected to CTF and C-PTF loading as well as monotonic loading, which is also observed from experimental and simulated response of all tested notched specimens in this study. This is important from an engineering viewpoint: although there are no obvious surface cracks, the components may fracture due to internal crack initiation.

In the different loading case, the damage in the center of base metal specimen versus loading displacement is illustrated in Fig. 14. It shows that the damage evolution curve in the first cycle under cyclic loading is coincided with that under monotonic tension loading. The main reason is that the same hardening model parameters were used in different loading condition and the cyclic cumulative damage model (see Eq. (7)) can also degenerate to the damage model under monotonic loading condition, as
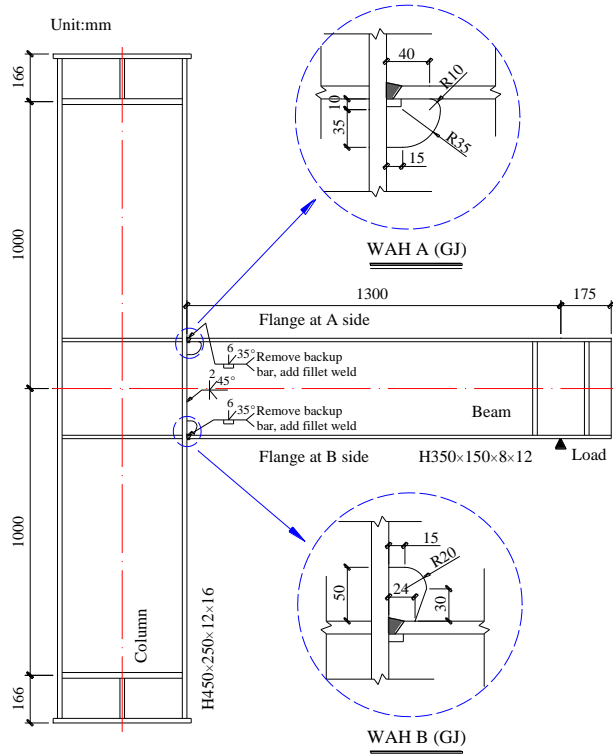
Fig. 15 Geometries and weld details of GJ beam-column welded joint (Tong *et al.* 2016)

aforementioned in Section 3. For C-PTF loading and monotonic loading, it is likely that dislocation density increases during the tension-compression process because of plastic deformation what is comparable with cold working process. The higher dislocation density results in a disability of the dislocation movement, thereby cyclic hardening behavior appears, in addition a lower ductility and an earlier failure were observed in C-PTF loading than that in monotonic tension loading, as shown in Fig. 14.

5. ELCF fracture prediction of beam-column welded joints

5.1 Experimental data

In order to verify the proposed cumulative damage model, it was applied to predict ELCF behavior of beam-column welded joints (Tong *et al.* 2016). The welded joint was single-side beam-column assemblies which were representative of exterior beam-column welded joints. The tested welded joint shown in Fig. 15 is named as GJ joint made of a Q345 H450×250×12×16 mm column and a Q345 H350×150×8×12 mm beam. By using of a full joint penetration groove weld, the beam flange and web were connected to column flange. Details of the complete groove welds are shown in Fig. 15. According to Chinese code for seismic design of buildings (2010), two different weld access hole (WAH) were adopted in the welded joints, namely WAH A and WAH B. Meanwhile, the backup bar was used at beam flange to ensure the penetration welding quality well, and it was removed and a fillet weld was
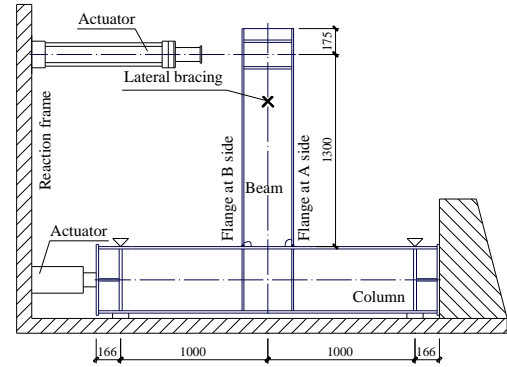

Fig. 16 Extremely low cycle fatigue test of beam-column welded joint (Tong *et al.* 2016)
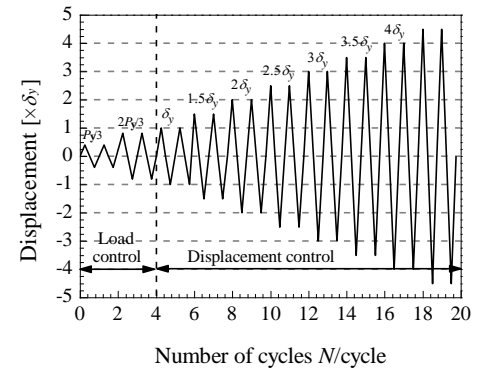

Fig. 17 Schematic plot of loading history imposed on joint GJ-H (Tong *et al.* 2016)

added.

As depicted in the test setup in Fig. 16, the column was placed horizontally and an actuator mounted in a self-balancing reaction frame imposed the cyclic loads at the beam tip. Axial compression ratio of steel column was kept the constant value 0.1 in the test, while the predetermined symmetric cyclic displacement was imposed on the beam tip by the actuator. GJ-H joint was tested quasi-statically under variable amplitude cyclic loading, as shown in Fig. 17. The yield displacement δ_y=16.5 mm and yield load P_y=207.2 kN were obtained from the monotonic loading test of GJ joint (Tong *et al.* 2016). GJ-C joint was tested under constant amplitude cyclic loading, where the displacement amplitude was $1.5\delta_y$. Different displacement loading schemes were adopted to validate the applicability of the proposed cumulative damage model in predicting ELCF failure under different loading conditions. The load and displacement at beam tip of tested welded joints were measured in the experiments and are shown later in Fig. 21. As shown in Table 3, the experimental data of both beam-column welded joints are summarized, where P_u and δ_u is the ultimate load and ultimate displacement at beam tip, respectively.

5.2 Numerical modeling

There full-scale numerical models of tested beam-column welded joints were established by software ABAQUS with eight node complete integral linear solid

Table 3 Test results (Tong *et al.* 2016) and prediction of joints

Joint No.	Test					Prediction				
	Ultimate load P_u/kN	Ultimate displacement δ_u/mm	N_i /cycle	N_f /cycle	Crack location	Ultimate load P_{tt}/kN	Ultimate displacement δ_u/mm	N_i /cycle	N_f /cycle	Crack location
GJ-H	257.6	33	8	11	WAH B	280.5	33	9	11	WAH B
GJ-C	253.3	-	5	9	WAH B	266.2	-	7	9	WAH B

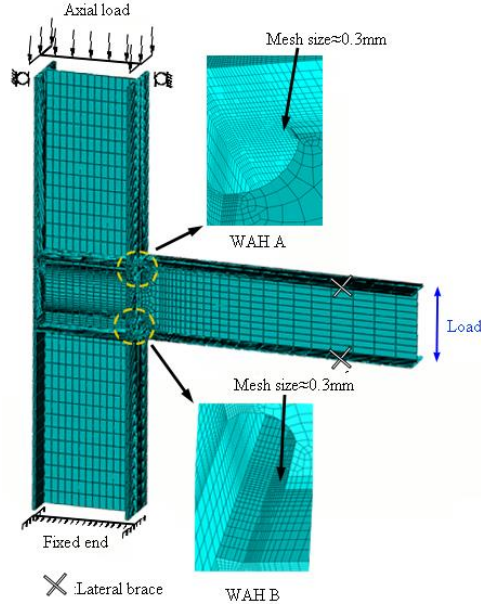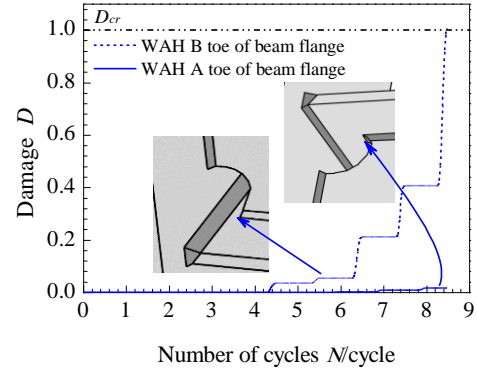Note: N_i is the load cycles corresponding to onset of crack. N_f is the total fatigue life.

Fig. 18 Finite element model of GJ joint

(a) GJ-H

(b) GJ-C

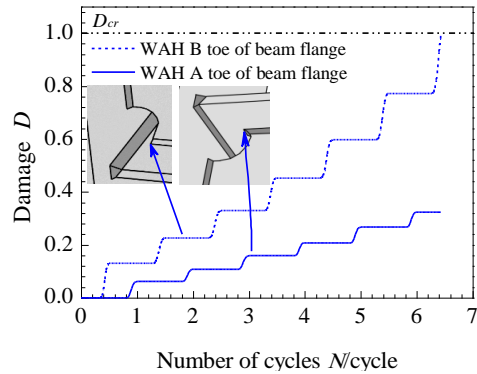Fig. 19 Damage evolution law at the WAH toe of beam flange

elements as illustrated in Fig. 18. For a standard computer, the numerical calculation will consume a great deal of time and energy if taking the characteristic length of steel as the global mesh size of finite element model of joints, thus the finer mesh size is only used in the critical locations with fracture potential. As shown in Fig. 18, appropriate displacement constraints were assigned at the nodes to simulate actual boundary conditions. Moreover, the load was applied at the beam tip during the analysis, which was identical to the testing loading histories. Hardening model parameters and damage parameters of base metal and weld metal (see Table 2) were considered in the simulation of ELCF failure of beam-column welded joints.

5.3 Numerical results

The damage evolution law at different locations of beam-column welded joint was computed, and it is found from the FEA results that the possible locations in the welded joint where fracture first occurred are at the WAH toe of beam flange. Comparisons are made at these locations as shown in Fig. 19. It shows that damage increases cyclically with the number of loading cycle. Obviously, for joint GJ-H and joint GJ-C, damage at WAH B toe of beam flange is apparently higher than that at WAH A toe of beam flange, consequently, the first crack is observed at the WAH B toe of beam flange, which are consistent with the test results (Tong *et al.* 2016).

For structural fracture prediction, whether the numerical modeling can represent the predominant characteristics of fracture process is intensely important. For joint GJ-H and joint GJ-C, the fracture process obtained by proposed cumulative damage model is compared with the fracture process as observed during the experimentation in Fig. 20. In the case of joint GJ-H, crack initiation is trigger at the toe of WAH B and then it firstly propagated along the thickness of beam flange from internal surface to external surface. When crack extended through the flange thickness, it would propagate along the width direction of beam flange from the center to the edge quickly, and finally causing the rupture of beam flange. From the comparison between test and predicted results, it can be found that the simulated response is able to accurately capture the key failure feature of joint GJ-H. As for joint GJ-C, the development process of crack at the beam flange is similar to that of joint GJ-H, and the predicted fracture process is also consistent with the observed fracture mode in the experiment as indicated in Fig. 20.
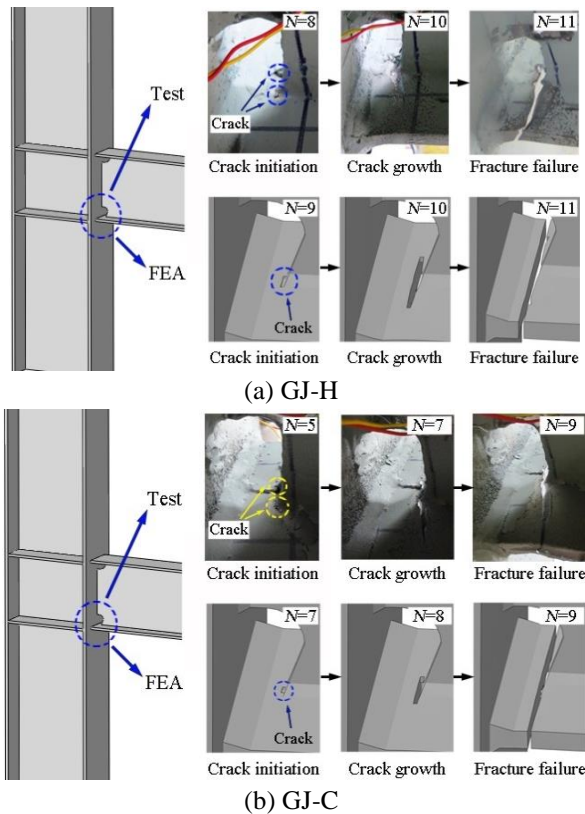
(a) GJ-H

(b) GJ-C

Fig. 20 Comparison of tested fracture process and predicted fracture process

(a) GJ-H

(b) GJ-C

Fig. 21 The predicted and tested load vs. displacement relationship at beam tip

The predicted load-displacement curves based on the proposed cumulative damage model in comparison with the experimental results for GJ-H and GJ-C joint are provided in Fig. 21. The crack onset points are indicated in the load-displacement curves, and it shows that the load does not drop suddenly once crack initiated, which is also observed in test results (Tong *et al.* 2016) and predicted results. Using the conventional elastic-plastic FEA the plastic behaviors of ELCF tests can be predicted up to the failure initiations. However, after failure initiation, the predicted results deviate from experimental data, as the conventional analysis cannot simulate crack propagation. As shown in Fig. 21, it indicates that the load-displacement behavior before crack initiation is satisfactorily represented by FEA incorporating cumulative damage model. In addition, the load degradation resulted from crack propagation is also well captured in the numerical simulation.

Table 3 summarizes and compares the test and predicted results, in which the cycles with the onset of cracking and total fatigue life as well as crack locations are compared. It indicates that the numerical results using the proposed cumulative damage model shows close agreement with the corresponding test results under extremely low cyclic loading. And the predicted result slightly overestimates the loading cycles corresponding to crack initiation. This overestimation may be due to no damage accumulation as the stress triaxiality below -1/3 assumed by the cumulative damage model, which may underestimate the damage cumulated rate under extremely low cyclic loading when the stress triaxiality is less than -1/3. However, these errors
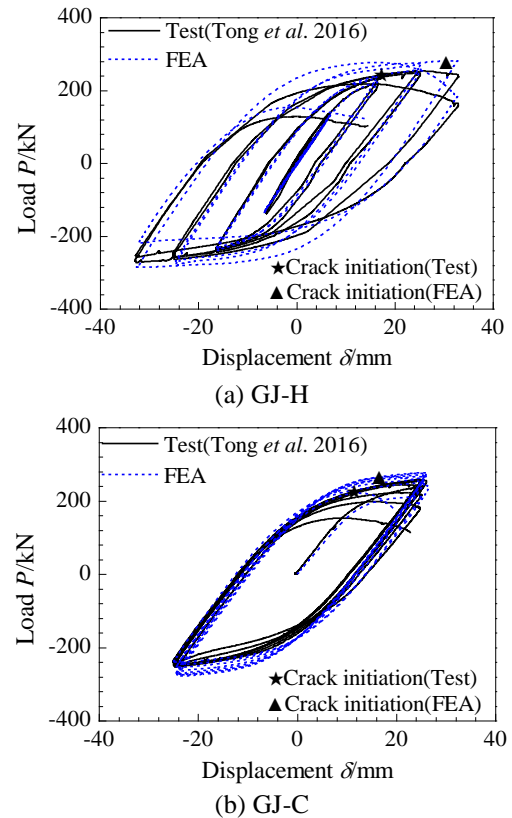
appear to be accepted compared to prediction of classical fatigue. Therefore, the cumulative damage model is able to be used to predict ELCF life of beam-column joints under constant amplitude and various amplitude cyclic loading.

6 Conclusions

In this study, a numerical methodology based cumulative damage model is proposed to simulate ductile fracture of structural steel. The model, extended from the case of monotonic loading, supposes that no damage will accumulate as stress triaxiality below -1/3, which can be applied to predict ductile fracture of structure steels under monotonic loading and extremely low cyclic loading.

There were two important parameters in the damage model to be determined. A number of notched coupon specimens previously tested under different loading conditions were selected to calibrate the parameters. For all the tested notched specimens, the cumulative damage model indicates that failure location is in the center of specimens, which agrees with test results.

The cumulative damage model was examined on full-scale beam-column welded joints. The simulated response shows that onset of crack is at the welded access hole toe of beam flange, and crack extends through the thickness of beam flange, then grows rapidly along the width direction of beam flange from the center to the edge and eventually lead to the rupture of the joints. From the comparison between experiment and simulation, it is found that the

predictions coincide with the test results exactly, which verify the applicability of the model.

Though the damage model predicts cracking behavior of welded joints with good accuracy, there are some limitations of the proposed damage model. The cumulative damage model based on the Rice-Tracy type model is suitable for the tensile stress-dominant failure, which may not well predicted the shear stress-dominant failure. Thus further improvement of the proposed damage model may be required to consider a large variety of stress conditions in future work.

Acknowledgements

References

Amiri, H.R., Aghakouchak, A.A., Shahbeyk, S. and Engelhardt, M.D. (2013), "Finite element simulation of ultra low cycle fatigue cracking in steel structures", *J. Constr. Steel Res.*, **89**, 175-184.

Bao, Y. and Wierzbicki, T. (2004), "On fracture locus in the equivalent strain and stress triaxiality space", *Int. J. Mech. Sci.*, **46**(81), 81-98.

Bao, Y. and Wierzbicki, T. (2005), "On the cut-off value of negative triaxiality for fracture", *Eng. Fract. Mech.*, **72**(7), 1049-1069.

Besson, J. and Guillemer-Neel, C. (2003), "An extension of the Green and Gurson models to kinematic hardening", *Mech. Mater.*, **35**(1-2), 1-18.

Besson, J., Steglich, D. and Brocks, W. (2001), "Modeling of crack growth in round bars and plane strain specimens", *Int. J. Solid. Struct.*, **38**(46-47):8259-8284.

Bleck, W., Dahl, W., Nonn, A., Amlung, L., Feldmann, M., Schäfer, D. and Eichler, B. (2009), "Numerical and experimental analyses of damage behaviour of steel moment connection", *Eng. Fract. Mech.*, **76**(10), 1531-1547.

Bonora, N. (1997), "A nonlinear CDM model for ductile failure", *Eng. Fract. Mech.*, **58**(1), 11-28.

Chao, S., Khandelwal, K. and El-Tawil, S. (2006), "Ductile web fracture initiation in steel shear links", *J. Struct. Eng.*, **132**(8), 1192-1200.

Code for seismic design of buildings (2010), GB 50011-2010, China Architectura & Building Press, Beijing.

Dufailly, J. and Lemaitre, J. (1995), "Modeling very low cycle fatigue", *Int. J. Damage Mech.*, **4**(2), 153-170.

Hancock, J.W. and Mackenzie, A.C. (1976), "On the mechanisms of ductile failure in high-strength steels subjected to multi-axial stress-states", *J. Mech. Phys. Solid.*, **24**(s2-3), 147-160.

Huang, X., Tong, L., Zhou, F. and Chen, Y. (2013), "Prediction of fracture behavior of beam-to-column welded joints using micromechanics damage model", *J. Constr. Steel Res.*, **85**, 60-72.

Kamaya, M. (2010), "Fatigue properties of 316 stainless steel and its failure due to internal cracks in low-cycle and extremely

low-cycle fatigue regimes", *Int. J. Fatigue*, **32**(7), 1081-1089.

Kanvinde, A.M. and Deierlein, G.G. (2006a), "Void growth model and the stress modified critical strain model to predict ductile fracture in structural steels", *J. Struct. Eng.*, **132**(12), 1907-1918.

Kanvinde, A.M. and Deierlein, G.G. (2006b), "Prediction of ductile fracture in steel connections using SMCS criterion", *J. Struct. Eng.*, **132**(2), 171-181.

Kanvinde, A.M. and Deierlein, G.G. (2007), "Cyclic void growth model to assess ductile fracture initiation in structural steels due to ultra low cycle fatigue", *J. Struct. Mech.*, **133**(6), 701-712.

Kanvinde, A.M. and Deierlein, G.G. (2008), "Validation of cyclic void growth model for fracture initiation in blunt notch and dogbone steel specimens", *J. Struct. Eng.*, **134**(9), 1528-1537.

Kiran, R. and Khandelwal, K. (2014), "Gurson model parameters for ductile fracture simulation in ASTM A992 steels", *Fatigue Fract. Eng. Mater. Struct.*, **37**(2), 171-183.

Kiran, R. and Khandelwal, K. (2015), "A micromechanical cyclic void growth model for ultra-low cycle fatigue", *Int. J. Fatigue*, **70**, 24-37.

Kuroda. M. (2002), "Extremely low cycle fatigue life prediction based on a new cumulative fatigue damage model", *Int. J. Fatigue*, **24**(6), 699-703.

Kuwamura, H. (1998), "Fracture of steel during an earthquake-state-of-the-art in Japan", *Eng. Struct.*, **20**(4-6), 310-322.

Leblond, J.B., Perrin, G. and Devaux, J. (1995), "An improved Gurson-type model for hardenable ductile metals", *Eur. J. Mech. A*, **14**(4), 499-527.

Li, L., Wang, W., Chen, Y. and Lu, Y. (2015), "Effect of beam web bolt arrangement on catenary behaviour of moment connections", *J. Constr. Steel Res.*, **104**, 22-36.

Liao, F.F., Wang, W. and Chen, Y.Y. (2012), "Parameter calibrations and application of micromechanical fracture models of structural steels", *Struct. Eng. Mech.*, **42**(2), 153-174.

Mackenzie, A.C., Hancock, J.W. and Brown, D.K. (1977), "On the influence of state of stress on ductile failure initiation in high strength steels", *Eng. Fract. Mech.*, **9**(1), 167-188.

Mahin, S.A. (1998), "Lessons from damage to steel buildings during the Northridge earthquake", *Eng. Struct.*, **20**(4), 261-270.

Myers, A.T. (2009b), "Testing and probabilistic simulation of ductile fracture initiation in structural steel components and weldments", Stanford University, California.

Myers, A.T., Kanvinde, A.M., Deierlein, G.G. and Fell, B.V. (2009a), "Effect of weld details on the ductility of steel column baseplate connections", *J. Constr. Steel Res.*, **65**, 1366-1373.

Nip, K.H., Gardner, L., Davies, C.M. and Elghazouli, A.Y. (2010), "Extremely low cycle fatigue tests on structural carbon steel and stainless steel", *J. Constr. Steel Res.*, **66**(1), 96-110.

Pironi, A. and Bonora, N. (2003), "Modeling ductile damage under fully reversed cycling", *Comput. Mater. Sci.*, **26**, 129-141.

Pironi, A., Bonora, N., Steglich, D., Brocks, W. and Hellmann, D. (2006), "Simulation of failure under cyclic plastic loading by damage models", *Int. J. Plast.*, **22**(11), 2146-2170.

Rice, J.R. and Tracey, D.M. (1969), "On the ductile enlargement of voids in triaxial stress fields", *J. Mech. Phys. Solid.*, **17**(3), 201-217.

Ristinmaa, M. (1997), "Void growth in cyclic loaded porous plastic solid", *Mech. Mater.*, **26**(4), 227-245.

Rousselier, G. (1987), "Ductile fracture models and their potential in local approach of fracture", *Nucl. Eng. Des.*, **105**(1), 97-111.

Steglich, D., Pironi, A., Bonora, N. and Brocks, W. (2005), "Micromechanical modelling of cyclic plasticity incorporating damage", *Int. J. Solid. Struct.*, **42**(2), 337-351.

Tong, L., Huang, X., Zhou, F. and Chen, Y. (2016), "Experimental and numerical investigations on extremely-low-cycle fatigue fracture behavior of steel welded joints", *J. Constr. Steel Res.*,

119, 98-112.

Xue, L. (2008), "A unified expression for low cycle fatigue and extremely low cycle fatigue and its implication for monotonic loading", *Int. J. Fatigue*, **30**(10-11), 1691-1698.

Zhou, H., Wang, Y., Shi, Y., Xiong, J. and Yang, L. (2013), "Extremely low cycle fatigue prediction of steel beam-to-column connection by using a micro-mechanics based fracture model", *Int. J. Fatigue*, **48**(2), 90-100.

Zhou, H., Wang, Y., Yang, L. and Shi, Y. (2014), "Seismic low-cycle fatigue evaluation of welded beam-to-column connections in steel moment frames through global-local analysis", *Int. J. Fatigue*, **64**(7), 97-113.

CC